Arctic and Antarctic Diurnal and Seasonal Variations of Snow Albedo from Multi-year BSRN Measurements

Xianwei Wang and Charles S. Zender

Department of Earth System Science, University of California, Irvine, USA

Corresponding Author: Xianwei Wang

Email: xianweiw@uci.edu; xianwei8.wang@gmail.com

Tel: 949-824-1571

Fax: 949-824-3874

Abstract

This study analyzes diurnal and seasonal variations of snow albedo at four BSRN stations in the Arctic and Antarctica from 2003 to 2008 to elucidate similarities and differences in snow albedo diurnal cycles across geographic zones and to assess how diurnal changes in snow albedo affect the surface energy budget. At the seasonal scale, the daily albedo for the perennial snow in Antarctica (stations SPO and GVN) has a similar symmetric variation with solar zenith angle (SZA) around the austral summer; the daily albedo for the seasonal snow in Arctic (stations BAR and NYA) tends to decrease with SZA decrease from winter to spring before snow starts melting. At the hourly scale, each station shows unique diurnal cycles due to different processes that affect snow albedo such as cloud cover, snow metamorphism, SZA, solar azimuth angle (SAA) and surface features. Cloud escalates the snow albedo at all four stations by shifting solar radiation to visible wavelengths, and diminishes the diurnal variation by diffusing incident solar radiation. The 24-hour mean snow albedo is higher on cloudy than clear days by 0.02 at SPO (December) and BAR (May), 0.05 at GVN (December) and 0.07 at NYA (April). The diurnal variation (max-min) (0.06) of snow albedo at SPO shows strong effects of snow surface structures, e.g., wind-channeled sastrugi, which also contribute to the large (0.1-0.2) diurnal variation at GVN and NYA. The asymmetric diurnal variation of snow albedo at GVN and BAR is consistent with snow metamorphism. Near the melting point temperature, melt-freeze cycles exceed cloud impacts and dominate the diurnal variation of snow albedo. All these diurnal variations indicate that the satellite-measured clear sky snow albedo usually underestimates the average all-sky snow albedo. Further, sun-synchronous satellite's daily instantaneous observations undersample the diurnal variation of snow albedo, which causes biases in daily and monthly mean albedo products constructed from them.

Key Words: Snow Albedo; Diurnal Variation; BSRN; Arctic; Antarctica

1. Introduction

The shortwave (SW) broadband snow albedo (referred to as snow albedo hereafter) is of great interest to climate studies in that it describes the net solar radiation flux at the snow surface and small errors or changes in its value represent large fractional changes in absorbed solar radiation (ASR) and in the overall heat budget at the snow surface (Carroll and Fitch, 1981; Pirazzini, 2004). Although snow albedo dominates the surface energy budget of the Arctic and Antarctic (Hall, 2004), the remote location, harsh conditions, extensive cloud cover, and large solar zenith angles in these regions combine to hinder the development of climatological data records of snow albedo. As a result, little is known about the climatological diurnal cycle of polar snow albedo, and its geographic and seasonal variations. Recently, the Baseline Surface Radiation Network (BSRN) has accumulated sufficiently long time series of high quality, high frequency radiometric data to allow climatological characterization of the diurnal cycle of snow albedo. This study analyzes diurnal and seasonal variations of snow albedo at four BSRN stations in the Arctic and Antarctica from 2003 to 2008 to elucidate similarities and differences in snow albedo cycles across geographic zones and to assess how changes in snow albedo affect the surface energy budget.

Snow has high reflectance in visible (VIS) and low reflectance in infrared (IR) wavelengths. Snow bi-directional reflectance varies strongly with solar zenith angle (SZA) and viewing geometry (Wiscombe and Warren, 1980; Salomon et al., 2006). However, climate models typically represent only the zenith, not the azimuthal dependence of snow albedo (Roesch, 2006). Snow directional-hemispherical reflectance has a larger magnitude of increase with SZA in IR (1.03 μm) than in VIS (0.55 μm) wavelengths (Schaepman-Strub et al., 2006). Snow albedo integrates the angular and spectral variations of snow reflectance over the entire

90 solar spectrum (SW) wavelengths, and has strong diurnal and seasonal cycles depending on both
91 atmospheric and surface conditions (Pirazzini, 2004).

92 Dry snow albedo depends on internal snow characteristics such as snow grain size and
93 shape, snowpack depth, surface roughness, light-absorbing impurities, and on external factors,
94 including the SZA and solar azimuth angle (SAA), the spectral distribution of solar radiation,
95 atmospheric conditions (clouds, water vapor and aerosol, etc.), and shadowing (Warren, 1982;
96 Pirazzini, 2004). Observations confirm the predictions of models that, all else being equal, snow
97 albedo increases with decreasing snow grain size and with increasing SZA (Warren and
98 Wiscombe, 1980; Jin et al., 2003). For example, increasing SZA from 0° to 60° increases clear
99 sky snow albedo of a model snowpack from 0.75 to 0.78 (Wang and Zender, 2010a). Falling
100 snow often consists of fine and/or multi-faceted snow grains and has higher albedo immediately
101 after snowfall (Grenfell et al., 1994). For example, doubling the effective radius of ice crystals
102 from 100 to 200 μm, as can occur during a few days of isothermal aging in warm conditions,
103 may reduce albedo from 0.85 to 0.80 (Flanner and Zender, 2006; Taillandier et al., 2007).

104 Cloud cover affects both the spectral distribution of solar irradiance and the effective
105 SZA, resulting in an increase of snow albedo of 5-10% from its value in clear sky in Antarctica
106 (Wiscombe and Warren, 1980; Pirazzini, 2004). Small amounts of strongly absorbing impurities,
107 especially soot, although dust and volcanic ash can also be effective in larger quantities, lower
108 snow albedo mainly in the VIS spectral regions ($\lambda < 0.9$ μm) where absorption by pure snow is
109 weakest. Light-absorbing impurities within snow cause the greatest reductions in albedo for
110 coarse-grained snow (Warren and Wiscombe, 1980; Warren, 1982). When the sun azimuth is
111 perpendicular to the long axis of the wind channeled surface features known as sastrugi at the
112 South Pole, snow albedo is reduced as much as 4% from its value when the sun azimuth is

parallel to the sastrugi (Carrol and Fitch, 1981).

Snow albedo dynamically changes because of its changing internal properties and external environments. Under overcast skies, surface insolation is diffuse and nearly isotropic, so the effects of SZA and SAA on albedo are negligible, and when snow metamorphism is slow then the snow albedo remains rather constant throughout the day (Pirazzini, 2004). During clear days, snow albedo undergoes large variations due to shadowing, snow metamorphism and changes in SZA and SAA. The diurnal variation (maximum - minimum) of snow albedo was measured as about 0.04 at the South Pole (Carrol and Fitch, 1981), and reaches up to 0.15 on the Antarctic coast (Pirazzini, 2004; Wuttke et al., 2006) and over sea ice in the Baltic Sea (Pirazzini et al., 2006). For a snowpack with mean albedo of 0.8, a diurnal albedo change of 0.10 represents a diurnal ASR change of 50%. This ASR change is significant for climate or surface process models, especially in seasonally snow covered regions where changes in ASR can accelerate the onset of snow melt and its attendant strong snow albedo feedbacks (Flanner et al., 2007). For comparison, the diurnal variation of surface albedo in a natural grassland (mean albedo of about 0.2) is 0.05 (Song, 1998), and could be up to 0.1 (or a ASR change of 12%) at a given SZA due to the formation of dew and reclined canopies by prevailing wind direction (Minnis et al., 1997).

Despite the numerous mechanisms besides SZA which can contribute to the diurnal cycle of snow albedo, methods for remote sensing of surface properties, estimation of clear-sky surface albedo (Brooks et al., 1986), and parameterization of surface albedo in atmospheric process and climate models (Briegleb and Ramanathan, 1982; Oleson et al, 2003) generally assume that the diurnal cycle of snow albedo depends only on SZA. In most radiation transfer models, the diurnal variation of surface albedo is assumed to be symmetric about solar noon and

forced by the diurnal variation of SZA (Song, 1998). Both regular and irregular changes in the surface state and environment can negate this assumption (Minnis et al., 1997; Pirazzini, 2004; Pirazzini, 2006). Consequently, sun-synchronous satellites should consider the diurnal variation of surface albedo or else risk biasing the monthly or daily mean values composed from measurements taken instantaneously once daily (Minnis et al., 1997).

Several studies analyze the diurnal variation of snow albedo, yet these studies are all short-term or experimental campaign measurements that focus on a single station/region (Carrol and Fitch, 1981; Pirazzini, 2004; Pirazzini, 2006; Wuttke et al., 2006; Meinander et al., 2008). To our knowledge, no studies have yet been conducted to examine and compare the climatological amplitude of snow albedo's diurnal and seasonal variation in both polar regions. Satellites provide near global coverage of snow albedo, though with temporal resolution too coarse and accuracy too low to capture diurnal variations. Fortunately, the long-term World Climate Research Programme (WCRP) Baseline Surface Radiation Network (BSRN) in the World Radiation Monitoring Center (WRMC) provides quality-controlled and consistent downwelling and upwelling solar irradiance measurements throughout the world, and thus offers us an chance to analyze the snow albedo's diurnal and seasonal variations in both polar regions with multi-year datasets. This study will, for the first time, systematically quantify and intercompare the climatological amplitude of snow albedo's diurnal and seasonal variations in the Arctic and Antarctic to elucidate similarities and differences in snow albedo cycles across geographic zones, and to assess how diurnal changes in snow albedo affect the surface energy budget.

2. Study Sites and Data

Four BSRN stations (Table 1) reside in the Arctic or Antarctic. Two stations (BAR and NYA) are in coastal areas of Barrow, Alaska, and Ny-Alesund Island, Spitsbergen. There are seasonally snow-covered for more than eight months from late September to early June. The other two stations are located on the coast (GVN) and at the South Pole (SPO) of Antarctica. Both are on the ice sheet and experience perennial snow. SPO is 2800 m above sea level while the other three coastal stations have elevation less than 50 m. NYA is located in a tundra mountain valley, while the other three stations are situated in flat and near uniform areas. These stations lie in areas with high surface reflectance, little grass (BAR) or no vegetation, and high SZA, and snow at the coastal stations, being also much warmer than SPO, are vulnerable to the warming atmosphere and adjacent oceans. Hence the long-term in situ BSRN measurements at these stations will help to increase our understanding of snow surface properties and their changes, and hence aid the improvement of surface albedo parameterizations and satellite albedo retrieval algorithms (McArthur, 2005).

The chief measurements used in this study are air temperature, SW broadband total downwelling (SWD) and upwelling (SWU) radiation fluxes, and the direct (DIR) and diffuse (DIF) components of the solar insolation. The air temperature at 2 m height is measured continuously by a thermometer with uncertainty of ±0.3 °C. The SW broadband solar radiation (SWD, SWU and DIF) are measured by two types of pyranometers. BAR and SPO use Eppley Precision Spectral Pyranometers (PSP). GVN and NYA use Kipp & Zonen CM11 and CM21 pyranometers. DIR at the four stations is measured by Eppley Normal Incidence Pyrheliometers (NIP). The four solar radiation variables are measured separately. DIR and DIF are relative quantities, and the sum of DIR and DIF does not equal to SWD. DIR and DIF are used to determine the clearness (or cloud index) of sky.

Both Kipp & Zonen CM1/21 and Eppley PSP applied at the BSRN stations are high performance research grade pyranometers. Their spectral response ranges are 0.3-2.8 μm for CM1/21 and 0.285-2.8 μm for PSP, which cover approximately 98% of the entire solar radiation at the earth surface. The measurement uncertainties are less than 2% or ±5 W/m^2 (whichever is greater) for SWD, 3% for SWU, 0.5% or ±1.5 W/m^2 for DIR, and 2% or ±5 W/m^2 for DIF when SZA is less than 75°; measurements with SZA larger than 80° are not used due to potential large errors related to the pyranometer's cosine-response quality and impacts of surface topography (McArthur, 2005; Kipp & Zonen, 2006). Thus, this study restricts its focus to measurements with SZA less than 75°.

The solar irradiances are sampled once per second and stored as one-minute averages. These one-minute mean irradiance and temperature data from 2003 to 2008 are retrieved from the WRMC-BSRN website at http://www.bsrn.awi.de/en/data/data_retrieval_via_pangaea/.

3. Data Processing

One-minute average irradiance data are processed into hourly means by a simple arithmetic average for values larger than 5 W/m^2, the SWD measurement uncertainty. These hourly data are further used to analyze the mean diurnal cycle within a month, which is the mean value during each hour from 0:00 to 23:00 within the 30/31 days of a month. Finally, the surface albedo is calculated using the mean SWU divided by the mean SWD at each hour. The clearness (or cloud) index in Equation (1) is a simplified normalized diffuse ratio variability test of clear sky (Long and Ackerman, 2000).

$$clr = \frac{DIR}{DIR + DIF} \qquad (1)$$

where clr is the clearness index of the sky and range from 0 (overcast) to 1 (clear). Clr is

normally less than 0.95 because of atmospheric aerosols. Hours with clr <0.3 are defined as cloudy sky. The mean clr value on cloudy days is less than 0.05, which implies that clouds, when present, are optically thick.

Our analyses are based on four time scales: 1) ten continuous diurnal cycles (hourly interval) including cloudy and clear sky days; 2) monthly mean diurnal cycles in December for SPO and GVN, in May for BAR, and in April for NYA when there is long/intense sunshine while snow still exists; 3) hourly minimum, mean and maximum based on the monthly mean diurnal variations from 2003 to 2008; and 4) the seasonal variation, which is the daily mean on each day from 2003 to 2008. The months (December, May, and April) selected for monthly mean diurnal cycles were chosen to sample the maximum forcing of snow albedo and its diurnal variation. The daily mean is the 24-hour mean with SWD and SWU larger than 5 W/m^2. All average calculations are using SWD and SWU, and the mean albedo is finally derived from the mean SWD and SWU. The diurnal variation here refers to the difference between the daily maximal value minus the minimal values.

4. Results

4.1 SPO

It is instructive to first examine data from SPO since the SZA there is nearly constant within a 24-hour period and, indeed, throughout December (Figure 1A). Hence the impact of SZA on the snow albedo diurnal cycle in December is negligible, though significant (~0.04 as SZA increases from 66° to 80°) at the seasonal scale (Figure 1D). Air temperatures at SPO are usually below -20°C, though occasionally reaches -14°C in the six years from 2003-2008 (Figure 1D). Hence the snow is perennially dry, and the snow metamorphism proceeds slowly

because of the extremely low air temperature (Figure 1A & B). However, the snow albedo at SPO on clear sky days still has a diurnal variation (of about 0.05) as shown in the first ten days in December 2003 (Figure 2), which reduces to about 0.035 in the monthly mean diurnal cycle in December 2003 (Figure 1A), and to about 0.03 in the multi-year mean diurnal cycle in December from 2003 to 2008 (Figure 1C). During clear sky days, the minimum snow albedo (Clr_min) in the diurnal cycle is around 0.85, and the maximum snow albedo (Clr_max) has a similar diurnal pattern with but larger variation than the mean (Clr_mean) snow albedo (Figure 1C). The mean snow albedo varies between 0.85 and 0.88. The strong diurnal cycles disappear during cloudy skies. With constant SZA and solar radiation and extreme low air temperature, such strong clear sky diurnal cycles (up to 0.06 in Figure 2) must be associated with SAA and snow surface features, such as snow dunes, ripples and sastrugi (Weller, 1969; Kuhn and Siogas, 1978; Carroll and Bruce, 1981). The supplementary figure (S.Fig.1) shows a photo of snow sastrugi at SPO. When SAA is parallel to the long axis and the sun faces the sastrugi slope, more solar radiation reflects back to the pyranometer, and increases the snow albedo by as much as 0.06 relative to when SAA is parallel to the long axis and the sun is opposite the slope (higher side) of the sastrugi (Pirazzini, 2004). The 12-hour intervals between the maximum and minimum snow albedo also match the relationship of SAA and sastrugi's orientation (Figure 2). The impact of sastrugi on the snow albedo is between the two extreme situations when SAA is between 0° and 180° and between 180° and 360° to the long axis of the sastrugi.

The diffusion of incident solar radiation by clouds reduces snow albedo at large SZA (>66°), such as at SPO, since diffuse radiation has an effective SZA of ~55° (Wiscombe and Warren, 1980; Warren, 1982). Clouds also shift the spectral distribution of the incident solar radiation towards the visible due to the high absorption of water vapor and liquid water in near

infrared wavelengths. Grenfell and Maykut (1977) show that the spectral shift effect exceeds the diffusion effect in most cases, and leads to a net increase in the integrated snow albedo (Grenfell and Maykut, 1977). Figure 1A confirms that snow albedo on cloudy days has higher values than on clear sky days. Clouds also diminish the impact of SAA and sastrugi on snow albedo's diurnal cycle by diffusing the incident solar radiation (Figure 1A and Figure 2). This supports the interpretation that the strong diurnal cycle of snow albedo at SPO is likely caused by snow sastrugi or other inhomogeneous surface features. Since the atmosphere at SPO is nearly transparent and only five days have thin cloud in December (Table 2), the diurnal cycle of snow albedo is dominated by the clear-sky patterns. At the daily scale, the mean snow albedo in December on cloudy days (0.88) is only 0.02 higher than on clear sky days (0.86), with a mean value of 0.87 in December for both clear and cloudy days.

4.2 GVN

GVN is on the coast of Queen Maud Land and the Weddell Sea, where cloudy days, snow fall and drifting snow are frequent (Pirazzini, 2004). The snow albedo has a diurnal asymmetry with larger values in the morning and smaller values in the afternoon (Figure 3A&C). This diurnal asymmetry also exists in other months from October to February (S.Fig.2.A4), and is consistent with other observations near this station (Pirazzini, 2004; Wuttke et al., 2006). The much lower albedo value before 04:00 (solar time) and after 19:00 are likely related to the instrument measurement errors because the pyranometer has poor cosine-response quality at SZAs larger than 75° for CM1/21 (McArthur, 2005; Kipp & Zonen, 2006). For instance, on clear sky days on 27, 28, 29, and 30 November, 2005 (Figure 4), a much lower snow albedo exists when SZAs exceed 75°. The air temperature is lower than -8°C, thus snow melting and

liquid water content in snow are negligible and cannot explain the low snow albedo values at such large SZAs and low air temperature. In contrast, when clouds are present on days 23, 24, 25 and 26 in the same month, the strong diurnal cycles disappear, and the snow albedo increases to a near constant value of ~0.85 for SZAs larger than 75°. Moreover, the asymmetry of snow albedo still exists under the lower air temperatures (< -15 °C) of October and February. This suggests that the diurnal cycles of snow albedo are related to snow surface features and SAA.

On December 15, SZA varies from 48° at noon to 86° at 23:00, while the snow albedo peaks at 0.83 from 04:00-06:00, then falls to 0.75 from 18:00-19:00 in a reliable SZA range of the pyranometer (Figure 4A). This is approximately a 12-hour difference between the maximum and minimum reliable albedo value. This 12-hour difference is co-incidental with the sun azimuth cycle, indicating that the diurnal asymmetry is associated with surface features and SAA. The larger SZA in the morning also contributes to a higher albedo. Meanwhile, snow metamorphism due to strong solar radiation and relatively high coastal air temperatures also contribute to the lower snow albedo in the afternoon. In summary, the diurnal asymmetry of the snow albedo implies that the impact of SZA on albedo (particularly in the afternoon) in diurnal cycles gives ways to other factors, such as snow surface features (sastrugi) and snow metamorphism. Nevertheless, in Figure 3D, the near symmetric distribution of the seasonal snow albedo is likely due to the symmetric distribution of SZAs on the seasonal timescale. A similar symmetric distribution of seasonal snow albedo also occurs in Greenland (Wang and Zender, 2010a&b).

Snow albedo at GVN is larger (0.06 at ~5:00 to 0.12 at ~18:00) on cloudy than clear sky days (Figure 3A&C, Figure 4). As mentioned earlier, clouds alter snow albedo by shifting the spectral distribution of surface insolation to visible wavelengths, where snow is more reflective.

The magnitude of spectral shifting is related to the amount and type of cloud and column water vapor. At SPO, the daily SWD difference (clear-cloud) between clear and cloudy days in December is 76 W/m^2 or 17% of SWD in clear sky, leading to 0.02 higher albedo on cloudy days than on clear days (Figure 1C and Table 2). At GVN, the daily SWD difference in December is 109 W/m^2 or 26% of SWD in clear sky, leading to 0.05 higher albedo on cloudy days (Figure 3C and Table 2). Clouds also diffuse insolation and diminish the effects of surface features (sastrugi) and SZA on the diurnal cycle of snow albedo. The nearly constant snow albedo on cloudy days (Figure 3A&C, Figure 4) further suggests that the diurnal asymmetry on clear sky days at GVN stems from snow surface features and snow metamorphism.

4.3 BAR

Snow at BAR usually begins to melt and disappear in June, and then accumulates again beginning in late September or October (Figure 6D). To examine the diurnal cycle of snow albedo, we calculate the hourly mean SWD and SWU for each hour within each month for clear and cloudy sky. We find similar results from 2003 to 2008 as illustrated for 2005 in Figure 5. The maximum forcing of snow albedo diurnal variations at BAR occurs in May, when snow still exists and receives strong insolation. During May, the 23 cloudy days have smaller (-23%) SWD, higher air temperature, and also higher snow albedo than the clear sky days (Figure 5ABC and Table 2). In contrast, the snow albedo has strong diurnal cycles on clear sky days, and only weak diurnal cycles on cloudy days, when clouds diffuse insolation and thus diminish the impact of SZA and snow surface features on snow albedo. The asymmetry of the diurnal cycle of snow albedo, which peaks near 06:00 and reaches nadir near 15:00, coincident with maximum air temperature, is consistent with darkening due to snow metamorphism and grain

growth on clear sky days with relatively higher temperature.

Figure 6 shows the first ten diurnal cycles of snow/surface albedo during the onset of snow melt in June, 2004, when the air temperature varies from -4 °C to 1 °C and the sun continuously hangs above the horizon. Snow albedo shows an asymmetric diurnal cycle, maximal in the morning and minimal in the late afternoon (15:00-18:00). Snow albedo recovers after 18:00, presumably due to refreezing when the air temperature drops below the freezing point. When the snow completely disappears on days 8, 9 and 10, the surface albedo has a symmetric diurnal cycle with a minimum value around noon, consistent with soil albedo dependence on SZA (Wang et al., 2005). In summary, snow albedo diurnal cycles at BAR seem mainly determined by snow metamorphism and melt-freeze cycles.

4.4 NYA

Snow at NYA disappears as early as May (Figure 7D) in some years, earlier than at BAR, hence April is the month of maximum snow forcing. The mean diurnal cycle of snow albedo in April (Figure 7A, B, C) has a near symmetric diurnal cycle on clear sky days, minimal at noon and maximal in both morning and afternoon. In April 2005 (Figure 7A), the clear sky snow albedo increases from 0.69 at noon to 0.81 in the morning and afternoon when SZA is ~80°. Snow metamorphism, when active, would be expected to reduce snow albedo preferentially during warm hours, and thus enhance diurnal asymmetry as suggested at BAR and GVN. The nearly symmetric diurnal cycle, low air temperature (< -5 °C) and small solar radiation variation (<350 W/m^2) all indicate that the impact of snow metamorphism on the diurnal cycle at NYA is small, and perhaps negligible. Other factors in addition to SZA, such as snow surface features (snow dunes, sastrugi, etc.) and/or shadowing, are required to explain the large clear sky diurnal

343 variations. Snow albedo is nearly constant and up to 0.12 higher on cloudy than clear days,
344 which are ~4 °C colder (Figure 7A).

345 The first ten diurnal cycles in May 2005 at NYA (Figure 8) include both clear and cloudy
346 days. On clear sky days 4, 5, 6 and 10, snow albedo shows symmetric diurnal cycles minimal at
347 solar noon. This is the only site of the four we examined where the diurnal cycle of snow albedo
348 matches most radiation transfer model assumptions: the diurnal variation of surface albedo is
349 symmetric and forced by the diurnal variation of SZA. However, the diurnal cycle is much
350 larger than models typically predict (Song, 1998; Wang and Zender, 2010). The large diurnal
351 variation (up to 0.2) of snow albedo suggests that snow surface features somehow amplify SZA
352 effects to create the large and symmetric diurnal cycles. On cloudy days 8 and 9, the snow
353 albedo is larger and nearly constant. Clouds exist over half of April, reduce SWD by 46%, and
354 increase snow albedo by 0.07 at the daily scale (Table 2).
355
356 **4.5 ASR Difference**

357 The diurnal variations observed at the four BSRN stations show that instantaneous
358 observations of snow albedo at certain times of a day (e.g., sun-synchronous satellite
359 measurements) will, if naively extrapolated to daily or longer timescale averages, lead to
360 systematic biases in the surface energy budget. To quantify the potential biases incurred by
361 extrapolating instantaneous albedos to time-mean albedos, we compare the difference between
362 the absorbed solar radiation (ASR_0) from the 24-hour mean SWD and SWU, and the ASR
363 derived from the 24-hour mean SWD and the instantaneous albedo within each hour (Figure 9).
364 The ASR difference ($ASR-ASR_0$) patterns are opposite to the diurnal cycles of snow albedo
365 (Figures 1A, 3A, 5A, and 7A). ASR differences vary from -20 to 12 W/m^2 at NYA, from -16 to 9

366 W/m^2 at BAR, from -7 to 20 W/m^2 at GVN, and from -6 to 6 W/m^2 at SPO. Taking the equatorial
367 overpass times of satellites Terra (10:30) and Aqua (13:30) as examples, the ASR difference at
368 10:30 is close to zero for BAR, and -3, -1, and 10 W/m^2 for SPO, GVN, and NYA, respectively;
369 the ASR difference at 13:30 is near zero for GVN, and 4, 5, and 6 W/m^2 for SPO, NYA and
370 BAR, respectively. The 24-hour mean ASR at NYA in April, BAR in May, at GVN and SPO in
371 December is 39, 65, 83 and 61 W/m^2 for clear sky, and 26, 51, 60 and 59 W/m^2 for the entire
372 month including clear and cloudy sky, respectively (Table 2).

373 Even under ideal conditions that satellite sensors could correctly measure snow albedo,
374 the satellite-measured albedo on clear-sky days is systematically lower than on cloudy days
375 (Figures 1AB, 3AB, 5AB, and 7AB). Thus, albedo parameterizations based on satellite
376 measurements may generate systematic errors in the surface energy budget for cloudy sky days,
377 particularly in the climate model. The magnitude of errors is dependent on the amount of cloud
378 and SWD. For instance, the integrated 24-hour mean ASR difference between clear sky and all
379 sky (ASR1 – ASR2) is 13 (50%), 14 (28%), 23 (38%) and 2 (2%) W/m^2 (Table 2) at NYA in
380 April, BAR in May, GVN and SPO in December, respectively. ASR1 is derived from the clear-
381 sky SWD and SWU. ASR2 is derived from the monthly mean SWD and SWU for both clear and
382 cloudy-sky. Recall that these are the months of maximum forcing by snow albedo at each
383 station. The monthly and annual mean diurnal cycles and ASR difference in each month for each
384 station are shown in supplementary figures (S.Fig. 2-5). The ASR differences generally increase
385 from winter to summer and decline from summer to winter. The magnitude of the annual ASR
386 difference is about one third maximum monthly ASR differences.
387

388 **5. Summary and Discussion**

The BSRN has made available to the community precise, consistent and interannual measurements of solar radiation around the world. We use these to investigate the diurnal and seasonal variations of snow albedo, and to elucidate the difference and similarities at four BSRN stations in the Arctic and Antarctic from 2003 to 2008. The two Arctic stations (NYA and BAR) experience seasonal snow cover, while the two Antarctic stations (GVN and SPO) are on the ice sheet and experience perennial snow cover. We examine the monthly mean diurnal cycle of, during periods of maximum snow albedo forcing, the early summer months of April at NYA and May at BAR, and the austral summer month of December at both GVN and SPO. Each station shows unique diurnal cycles due to regionally different factors that affect snow albedo, including cloudiness, SZA, SAA, surface features, snow metamorphism, and melt freeze cycles.

Clouds are a major factor in controlling the diurnal cycle of snow albedo at the four stations. Within a month, cloud cover varies from 5 days in December at SPO, to 23 days in May at BAR. Clouds reduce the daily SWD from 17% at SPO to 46% at NYA (Table 2). Clouds also have a diurnal cycle with more clear-sky days from hours 8:00 to 14:00 than in other periods at these stations. The diurnal cycle of cloud cover is most pronounced at NYA, where there are 16 clear-sky days from hours 9:00 to 15:00, with up to 8 clear-sky days more than at other hours (Table 2). Cloud alters the snow albedo through several ways. Clouds shift the solar radiation spectral distribution of surface insolation by backscattering to space more VIS than NIR radiation, which tends to reduce snow albedo, while simultaneously absorbing more NIR than VIS radiation which acts to increase snow albedo. In addition, multiple scattering of radiation between cloud and snow surface, aka the “snow/ice blink”effect, shifts solar insolation towards VIS wavelengths, thus increasing the snow albedo (Grenfell and Perovich, 2008). Gardner and Sharp (2010) show the net effect of cloud absorption, backscatter and multiple

412 scattering with the surface is to shift the surface insolation towards VIS wavelengths. This net
413 effect appears at all stations we examined, increasing snow albedo by 0.07, 0.02, 0.05 and 0.02
414 at NYA, BAR, GVN and SPO respectively on cloudy days relative to clear (Table 2).
415 Meanwhile, clouds diffuse direct solar insolation, reducing or eliminating the impact of snow
416 surface features, SZA and SAA on snow albedo, thus changing the diurnal cycle of snow albedo
417 (Pirazzini, 2004). Indeed, the snow albedo remains nearly constant on cloudy days (Figures 1A,
418 4A, 7A, 8A) at the four BSRN stations, also consistent with spectral measurements in January
419 2004 at GVN by Wuttke et al. (2006).
420 Snow metamorphism may be classified into equilibrium (or dry) metamorphism-rounds,
421 kinetic metamorphism-facets, and melt-freeze (or wet) metamorphism. Driving forces behind
422 snow metamorphism are macroscopic snow temperature gradients, and microscopic vapor
423 pressure gradients (e.g., Flanner and Zender, 2006). Dry metamorphism results in a net transfer
424 of water from small to large crystals, which reduces the specific surface area and thus albedo of
425 snow (e.g., Domine et al., 2006; Picard et al., 2009). Metamorphism proceeds exponentially
426 faster in warm (e.g., > -5 °C) than cold snow (e.g., < -10 °C), and comes to a virtual standstill at
427 -40 °C (Colbeck, 1983; Taillandier et al., 2007). Consistent with this behavior, the diurnal cycle
428 and the snow albedo at SPO remain nearly constant on cloudy days (Figure 1A) which are all at
429 extremely low air temperature (e.g., < -20 °C) and experience constant solar radiation (and thus
430 negligible temperature gradients) throughout the diurnal cycle. In contrast, at GVN and BAR
431 (Figures 3, 5), where afternoon air temperature exceeds -5 °C, the asymmetry of snow albedo
432 diurnal cycle is consistent with snow metamorphism. During the onset of snow melt in the first
433 six days of June 2004 at BAR (Figure 6), snow melt-freeze metamorphism clearly exceeds the
434 impact of cloud on snow albedo and dominates the snow albedo diurnal cycle.

SZA increases snow albedo because the increased path over which obliquely-incident photons interact with snow grains allows more multiple scattering and less penetration of and absorption by the snow surface (Wiscombe and Warren, 1980; Lucht, 1998; Flanner and Zender, 2006). The dependence of snow albedo on SZA is most distinct in April and May at NYA (Figures 7, 8), where snow albedo has the same diurnal symmetry as SZA. At the seasonal scale, the snow albedo at GVN and SPO has a symmetric dependence on SZA, minimal in summer and higher in spring and fall (Figures 1D, 3D). Such near-symmetric seasonal snow albedo around summer also occurs in Greenland (Wang and Zender, 2010a&b). At BAR and NYA, the seasonal snow albedo shows an increase trend with SZA, too (Figures 5D, 7D). However, at very large SZA (e.g., > 80°) the shadowing effect of an uneven snow surface can decrease the snow albedo. For example, on days 27-30, November, 2005 at GVN (Figure 4), the much lower snow albedo (< 0.7) when SZA>80° is consistent with a shadowing effect by an uneven snow surface in addition to the pyranometer's cosine-response error, and to the reduction of the effective SZA by long-path atmospheric (Rayleigh and aerosol) scattering.

Surface features effects on snow albedo are related to SZA, SAA and the orientation, surface slope and size of the features (e.g., sastrugi). SAA and sastrugi's orientation and slope determine the sign of the effects, while SZA and sastrugi's depth determine the magnitude. Snow albedo is greatest when the sun faces the reclined side and is parallel to the long axis of the surface feature. At SPO with constant SZA (67°) and negligible snow metamorphism (Figure 1-2), the diurnal cycle of snow albedo is very likely due to the snow sastrugi, consistent with the 0.06 diurnal variation of snow albedo attributable to sastrugi found earlier (Wiscombe and Warren, 1980; Carrol and Fitch, 1981). The about 12-hour difference between the maximum and minimum reliable albedo at GVN coincides with the diurnal cycle of SAA, indicating that

surface features and SAA also contribute to the diurnal asymmetry, in addition to snow metamorphism (Figures 3AC). At NYA (Figures 7AC, 8), surface features may also contribute to the large diurnal variation of snow albedo. However, at all locations the impact of sastrugi, SAA and SZA can be overwhelmed by the diffusing effects of overcast cloud.

At very large SZA (e.g., > 80°), the clear sky diffuse insolation increases due to atmospheric (Rayleigh and aerosol) scattering, thus the effective SZA becomes less than the real SZA, resulting in lower snow albedo (Wiscombe and Warren, 1980). At GVN (Figures 3, 4), the much lower snow albedo in clear sky at SZA > 80° is consistent with reduction in effective SZA by long-path scattering, in addition to the instruments' cosine-response error and the shadowing effects of uneven snow surfaces (Strahler et al., 1999; McArthur, 2005; Kipp & Zonen, 2006).

6. Conclusions

The snow albedo at the four BSRN stations in both the Arctic and Antarctica displays different magnitudes and patterns of diurnal variation. These diurnal variations are dominated by different factors at each station, and depend on dynamically changing snow properties and environmental conditions. Satellite measured clear sky snow albedos will be lower (and thus, if treated naively, underestimate) the all-sky snow albedo. One-time instantaneous observations also lead to systematic biases if snow albedo diurnal variations are neglected. Snow albedo is, at these BSRN stations, usually not symmetric around solar noon, though the solar noon albedo is most important because of the peak solar radiation. Sometimes, e.g., for the asymmetric snow albedo diurnal variation at SPO and GVN, snow albedo near solar noon does best represent the 24-hour mean snow albedo. In other locations like NYA, solar noon coincides with minimal snow albedo, consistent with most current climate model parameterizations. The local times

most representative of 24-hour mean snow albedo are 10:30, 11:30, 13:30 and 14:30 for BAR, SPO, GVN and NYA, respectively. The instantaneous forcing due to the difference between instantaneous albedo and the 24-hour mean albedo is up to 50% of ASR. Snow-atmosphere radiative transfer models and other snow models coupled to general circulation models should also consider the diurnal variation of snow albedo in order to better represent the consequent fast-timescale feedbacks, e.g., snow melt-albedo feedback.

Acknowledgments. We thank all the researchers who deploy, operate, and maintain the World Climate Research Programme (WCRP) Baseline Surface Radiation Network (BSRN) stations that provide the *in situ* measurements on air temperature, shortwave upwelling, downwelling, direct and diffuse solar radiation used here. Funding for this work is provided by NASA International Polar Year (IPY) Program, NASA NNX07AR23G, and by NSF OPP ARC-0714088.

References:

Briegleb, B.P. and V. Ramanathan. 1982. Spectral and diurnal variations in clear sky planetary albedo. *J. Climate Appl. Meteorol.*, 21, 1168–1171.

Brooks, D.R., E.F. Harrison, P. Minnis, J.T. Suttles and R.S. Kandel. 1986. Development of algorithms for understanding the temporal variability of the Earth's radiation balance. *Rev. Geophys.*, 24, 422–438.

Carroll, J.J. and B.W. Fitch. 1981. Effects of solar elevation and cloudness on snow albedo at the South Pole. *J. Geophys. Res.*, 86, 5271-5276.

Colbeck, S.C. 1983. Theory of metamorphism of dry snow. *J. Geophys. Res.*, 88, C9, 5475-5482.

Domine, F., R. Salvatori, L. Legagneux, R. Salzano, M. Fily and R. Casacchia. 2006. Correlation between the specific surface area and the short wave infrared (SWIR) reflectance of snow. *Cold Regions Science and Technology*, 46, 60-68.

Flanner, M. G. and C. S. Zender. 2006. Linking snowpack microphysics and albedo evolution, *J. Geophys. Res.*, 111(D12), D12208, doi:10.1029/2005JD006834.

Flanner, M.G., C.S. Zender, J.T. Randerson and P.J. Rasch. 2007. Present-day climate forcing and response from black carbon in snow. *J. Geophys. Res.*,112, D11202, doi:10.1029/2006JD008003.

Gardner, A.S. and M.J. Sharp. 2010. A review of snow and ice albedo and the development of a new physically based broadband albedo parameterization. *J. Geophys. Res.*, doi:10.1029/2009JF001444.

Grenfell, T.C. and D.K. Perovich. 2008. Incident spectral irradiance in the Arctic Basin during the summer and fall, *J. Geophys. Res.*, 113, D12117, doi:10.1029/2007JD009418.

Grenfell, T. C. and G. A. Maykut. 1977. The optical properties of ice and snow in the Arctic Basin. *J. Glaciol.*, 18, 445 – 463.

Hall, A. 2004. The role of surface albedo feedback in climate. *Journal of Climate*, 17, 1550-1568.

Jin, Y., C. B. Schaaf, C. E. Woodcock, F. Gao, X. Li, A. H. Strahler,W. Lucht and S. Liang . 2003. Consistency of MODIS surface bidirectional reflectance distribution function and albedo retrievals: 2. Validation. *J. Geophys. Res.*, 108(D5), 4159, doi:10.1029/2002JD002804.

Kipp & Zonen. 2006. CMP series pyranometer instruction manual. *Manual version: 0806.* January 4, 2010, online retrieved at: http://www.kippzonen.com/.

Kuhn, M. and L. Siogas. 1978. Spectroscopic studies at McMurdo, South Pole and Siple stations during the austral summer 1977-78. *Antarctic. J.U.S.*, 13, 178-179.

Long, C.N. and T.P. Ackerman. 2000. Identification of clear skies from broadband pyranometer measurements and calculation of downwelling shortwave clouds effects. *J. Geophys. Res.*, 105, 15609-15626.

Lucht, W., C. B. Schaaf and A. H. Strahler. 2000. An algorithm for the retrieval of albedo from space using semiempirical BRDF models, *IEEE Trans. Geosci. Remote Sens.*, 38, 977 – 998.

McArthur, L.J.B. 2005. World Climate Research Programme, Baseline Surface Radiation Network (BSRN). *WCRP-121, WMO/TD-NO.1274*. Online retrieved on Nov 17, 2009 at: http://www.bsrn.awi.de/en/other/publications/.

Meinander, O., A. Konku, K. Lakkala, A. Heikkilä, L. Ylianttila and M. Toikka. Diurnal variations in the UV albedo of arctic snow. 2008. *Atmospheric Chemistry and Physics*, 8, 6551-6563.

Minnis, P., S. Mayor, W.L. Smith, Jr., and D.F. Young. 1997. Asysmetry in the diurnal variation of surface albedo. *IEEE Transcations on Geoscience and Remote Sensing*, 35,No.4, 879-891.

Oleson, K.W., G.B. Bonan, C.B. Schaaf, F. Gao,Y. Jin and A.H. Strahler. 2003. Assessment of global climate model land surface albedo using MODIS data. *Geophys. Res. Lett.*, 30(8), 1443, doi:10.1029/2002GL016749.

Picard, D., L. Arnaud, F. Domine and M. Fily. 2009. Determining snow specific surface area from near-infrared reflectance measurements: Numerical study of the influence of grain shape. *Cold Regions Science and Technology,* 56, 10-17.

Pirazzini R. 2004. Surface albedo measurements over Antarctic sites in summer. *J. Geophys. Res.*, 109, D20118, doi:10.1029/2004JD004617.

Pirazzini,R., T. Vihma, M.A. Granskog and B. Cheng. 2006. Surface albedo measurements over sea ice in the Baltic Sea during the spring snowmelt period. *Annals of Glaciology*, 44, 7-14.

Roesch, A. 2006. Evaluation of surface albedo and snow cover in AR4 coupled climate models. *J. Geophys. Res.*, 111, D15111, doi:10.1029/2005JD006473.

Salomon, J.G., C.B. Schaaf, A.H. Strahler, F. Gao, Y. Jin. 2006. Validation of the MODIS bidirectional reflectance distribution function and albedo retrievals using combined observations from the Aqua and Terra platforms. *IEEE Transactions on Geoscience and Remote Sensing*, 44, 1555-1565, DOI:10.1109/TGRS.2006.871564.

Schaepman-Strub, G., M.E. Schaepman, T.H. Painter, S. Dangel and J.V. Martonchik. 2006. Reflectance quantities in optical remote sensing-definitions and case studies. *Remote Sensing of Environment,* 103, 27-42.

Song, J. 1998. Diurnal asymmetry in surface albedo. *Agriculture and Forest Meteorology*, 92, 181-189.

Taillandier, A.-S., F. Domine, W.R. Simpson, M. Sturm and T.A. Douglas. 2007. Rate of decrease of the specific surface area of dry snow: Isothermal and temperature gradient conditions. *J. Geophys. Res.*, 112, F03003, doi:10.1029/2006JF000514.

Strahler, A.H., J.P. Muller, W. Lucht, C.B. Schaaf, et al. 1999. MODIS BRDF/Albedo product: algorithm theoretical basis document. *MODIS Product ID: MOD43*, Version 5.0, April, 1999.

Wang, Z., M. Barlage, X. Zeng, R.E. Dickinson and C.B. Schaaf. 2005. The solar zenith angle dependence of desert albedo. *Geophys. Res. Lett.*,, 32, L0543, doi:10.1029/2004GL021835.

Wang, X. and C. Zender. 2010a. MODIS albedo bias at high zenith angle relative to theory and to in situ observations in Greenland. *Remote Sensing of Environment,* 114, 563-575, doi:10.1016/j.rse.2009.10.014.

Wang, X. and C. Zender. 2010b.Constraining MODIS snow albedo at large solar zenith angles: Implications for the surface energy budget in Greenland. *J. Geophys. Res.*, doi:10.1029/2009JF001436, in press.

Warren, S.G. 1982. Optical properties of snow. *Review of Geophysics and space Physics*, 20, 67-89.

Warren, S.G. and W.J. Wiscombe. 1980. A model for the spectral albedo of snow. II: snow containing atmospheric aerosols. *Journal of the Atmospheric Sciences*, 37, 2734-2745.

Weller, G.E. 1969. Radiation diffusion in Antarctic ice media. *Nature*, 221, 335-356.

Wiscombe, W.J. and S.G. Warren. 1980. A model for the spectral albedo of snow. I: pure snow. *Journal of the Atmospheric Sciences*, 37, 2712-2733.

Wuttke, S., G. Seckmeyer, and G. Kőnig-Lango. 2006. Measurements of spectral snow albedo at Neumayer, Antarctica. *Annales Geophysicae*, 24, 7-21.

Figure titles:

Figure 1. The monthly mean diurnal cycle of snow albedo and air temperature (A) and the shortwave broadband total downwelling and upwelling solar irradiance (B) for clear sky (26 days) and cloudy sky (5 days) at SPO in December, 2003; the multi-year mean diurnal cycle in December from 2003, 2006 and 2007 (C); the seasonal (daily mean from 2003, 2006 and 2007) variation of snow albedo at SPO (D). The SWD and SWU data in 2004, 2005 and 2008 are not used here because of instrumental problems.

Figure 2. Diurnal cycles in the first ten days of December, 2003, at SPO. "Clear" is the sky clearness or cloud index (0 is overcast sky) derived from Equation (1). The SZA in December at SPO is nearly constant at 67° with azimuth angles of 0° to 360°. The maximum air temperature during these ten days was below -20 °C.

Figure 3. The mean diurnal cycle of snow albedo and air temperature (A) and the shortwave broadband total downwelling and upwelling solar irradiance (B) for clear sky (12 days) and cloudy sky (19 days) at GVN in December, 2003; the hourly mean diurnal cycle in December from 2003-2008 (C); the seasonal (daily mean from 2003-2008) variation of snow albedo (D). The snow albedo values in clear sky days when SZA is larger than 75° (A) beyond two vertical lines are not reliable because of the pyranometer's cosine-response error at large SZAs.

Figure 4. Diurnal cycles of in situ snow albedo, air temperature, and cloud index in the last ten days of November, 2005, at GVN. "Clear" is the sky clearness or cloud index (0 is overcast sky, 1 is cloudless sky) derived from Equation (1). The SZA on November 25 at GVN varies from 49° at solar noon to 88° at 0:00.

Figure 5. The mean diurnal cycle of snow albedo and air temperature (A) and the shortwave broadband total downwelling and upwelling solar irradiance (B) for clear sky (8 days) and cloudy sky (23 days) at BAR in May, 2005; the hourly mean diurnal cycle in May from 2003-2008 (C); the seasonal (daily mean from 2003-2008) variation (D).

Figure 6. Diurnal cycles of in situ snow albedo, air temperature, and cloud index in the first ten days of June, 2004, at BAR. "Clear" is the sky clearness or cloud index (0 is overcast sky) derived from Equation (1). The SZA on June 5 varies from 49° at local noon to 85° at local 23:00. The sun is always above the horizon during this period.

Figure 7. The mean diurnal cycle of snow albedo and air temperature (A) and the shortwave broadband total downwelling and upwelling solar irradiance (B) for clear sky (13 days) and cloudy sky (17 days) at NYA in April, 2005; the hourly mean diurnal cycle in April from 2003-2008 (C); the seasonal (daily mean from 2003-2008) variation (D), and the daily values are derived from the 24-hour period when both SWD and SWU are larger than 5 W/m^2.

Figure 8. Diurnal cycles of in situ snow albedo, air temperature, and cloud index in the first ten days of May, 2005, at NYA. "Clear" is the sky clearness or cloud index (0 is overcast sky) derived from Equation (1). The SZA on May 5 varies from 62° at local noon to 85° at local 23:00. The sun is always above the horizon during this period.

Figure 9. The difference of absorbed solar radiation (ASR) in clear-sky days on the snow surface derived from the daily mean SWD and SWU (ASR_0) and from the daily mean SWD and one instantaneous albedo within each hour, which is assumed to represent the instantaneous albedo measurement from a sun-synchronous satellite. This instantaneous albedo also represents the daily albedo to assess the ASR difference for satellite's instantaneous measurements (ASR) versus the 24-hour mean value (ASR_0). The daily mean ASR at NYA in April, BAR in May, GVN and SPO in December is 39, 65, 83 and 61 W/m^2 for clear sky, and 26, 51, 60 and 59 W/m^2 for the entire month for clear and cloudy sky, respectively (Table 2). The two vertical green lines indicate the equatorial pass time of Terra and Aqua satellites that onboard MODIS instruments.

Table 1. Study sites in Arctic and Antarctica

Station ID	Area Name	Surface /topography Type	Elevation (m)	Latitude	Longitude
22 (BAR)	Barrow, Alaska, USA	tundra; flat, rural.	8	71.323	-156.607
11 (NYA)	Ny-Ålesund, Spitsbergen	tundra; mountain valley	11	78.925	11.950
13 (GVN)	Georg von Neumaye, Antarctica	iceshelf; flat, rural	42	-70.650	-8.250
26 (SPO)	South Pole, Antarctica	glacier, accumulation area; flat, rural	2800	-89.983	-24.799

Table 2. Mean (2003-2008) number of days at each hour for clear and cloudy skies, and the daily (24-hour) average in each month at four BSRN stations. The daily albedo1 and ASR1 are for clear and cloudy sky days separately, and the daily albedo2 and ASR2 are for both clear and cloudy sky days.

Stations	NYA		BAR		GVN		SPO	
Month	April		May		December		December	
Hour\sky	Clear	Cloud	Clear	Cloud	Clear	Cloud	Clear	Cloud
0	8	23	5	26	12	19	25	6
1	11	21	6	25	12	19	24	7
2	11	20	8	24	11	20	26	5
3	13	18	7	24	12	19	27	4
4	14	17	7	24	12	19	27	4
5	13	18	7	24	12	19	26	5
6	15	16	8	23	13	18	27	4
7	15	17	8	23	12	19	26	5
8	15	16	10	22	14	18	27	4
9	17	14	9	22	13	18	27	4
10	16	15	10	21	13	18	27	4
11	16	15	9	22	13	18	27	4
12	16	15	10	21	14	17	28	3
13	15	16	12	20	13	18	27	4
14	16	16	10	21	12	19	26	5
15	16	15	9	22	12	19	27	4
16	14	18	8	23	13	19	26	5
17	13	18	8	23	13	18	26	5
18	12	20	9	22	13	18	26	5
19	11	20	8	23	13	18	27	4
20	11	20	9	22	13	18	28	3
21	10	21	9	22	12	19	27	4
22	9	22	8	23	12	19	26	5
23	9	23	6	25	11	20	26	5
mean days	13	18	8	23	12	19	26	5
Daily SWD	159	86	300	231	417	308	446	370
SWD reduction (Clr-Cld)/Clr	73 (W/m^2)	46%	69	23%	109	26%	76	17%
Daily Albedo1	0.75	0.82	0.78	0.80	0.80	0.85	0.86	0.88
Daily Albedo2	0.78 (For all sky)		0.80		0.83		0.87	
Daily ASR1	39	16	65	45	83	45	61	43
Daily ASR2	26		51		60		59	

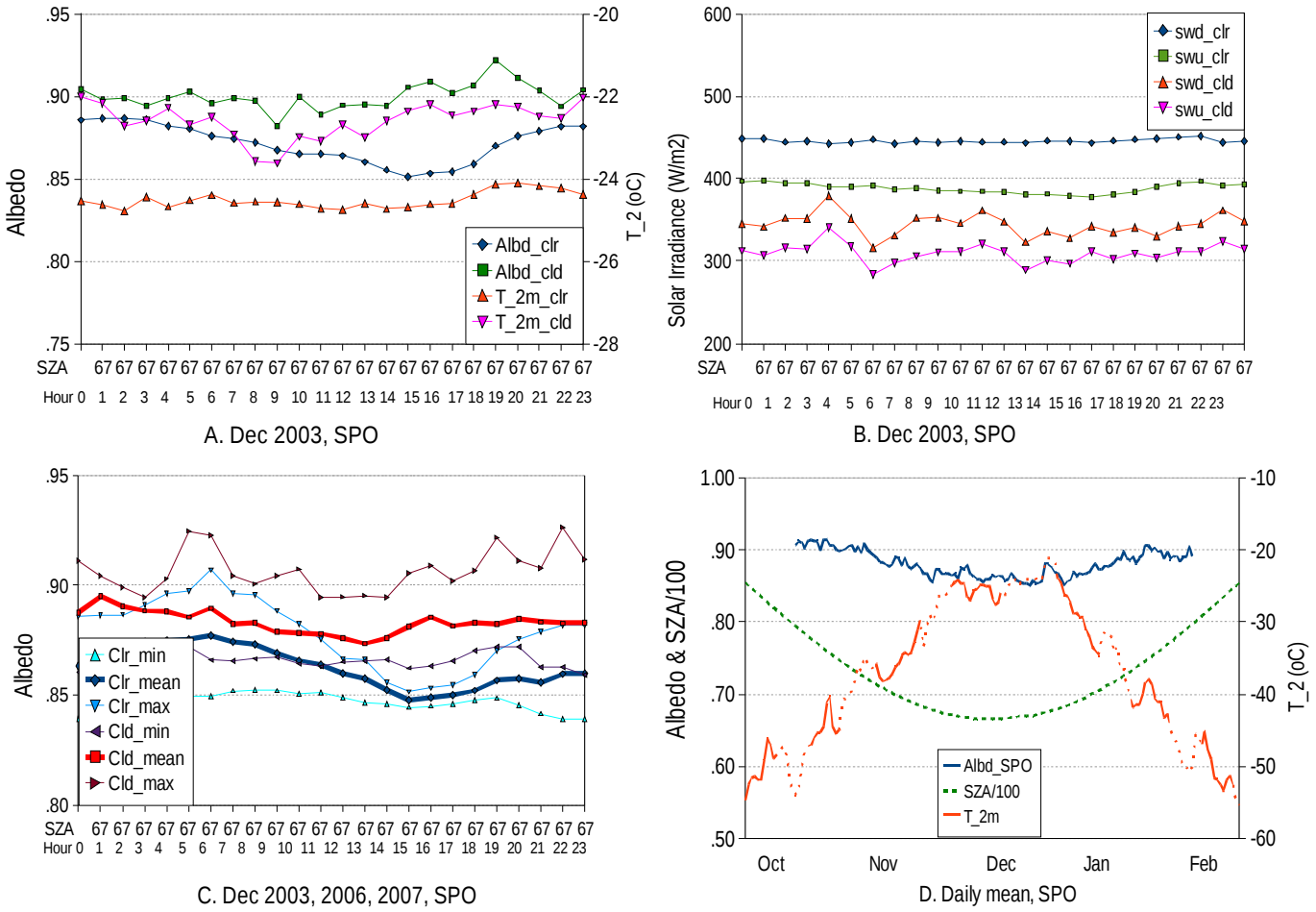

Figure 1. The monthly mean diurnal cycle of snow albedo and air temperature (A) and the shortwave broadband total downwelling and upwelling solar irradiance (B) for clear sky (26 days) and cloudy sky (5 days) at SPO in December, 2003; the multi-year mean diurnal cycle in December from 2003, 2006 and 2007 (C); the seasonal (daily mean from 2003, 2006 and 2007) variation of snow albedo at SPO (D). The SWD and SWU data in 2004, 2005 and 2008 are not used here because of instrumental problems.

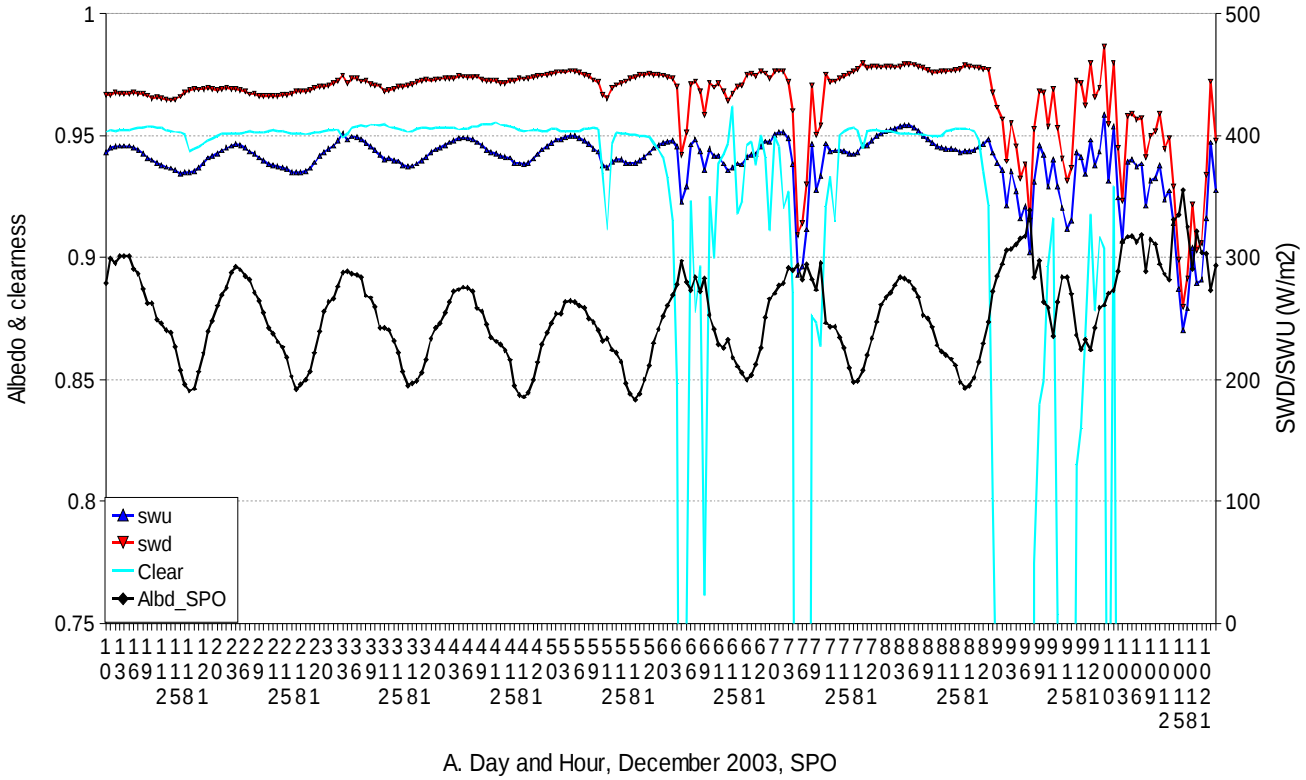

Figure 2. Diurnal cycles in the first ten days of December, 2003, at SPO. "Clear" is the sky clearness or cloud index (0 is overcast sky) derived from Equation (1). The SZA in December at SPO is nearly constant at 67° with azimuth angles of 0° to 360°. The maximum air temperature during these ten days was below -20 °C.

673

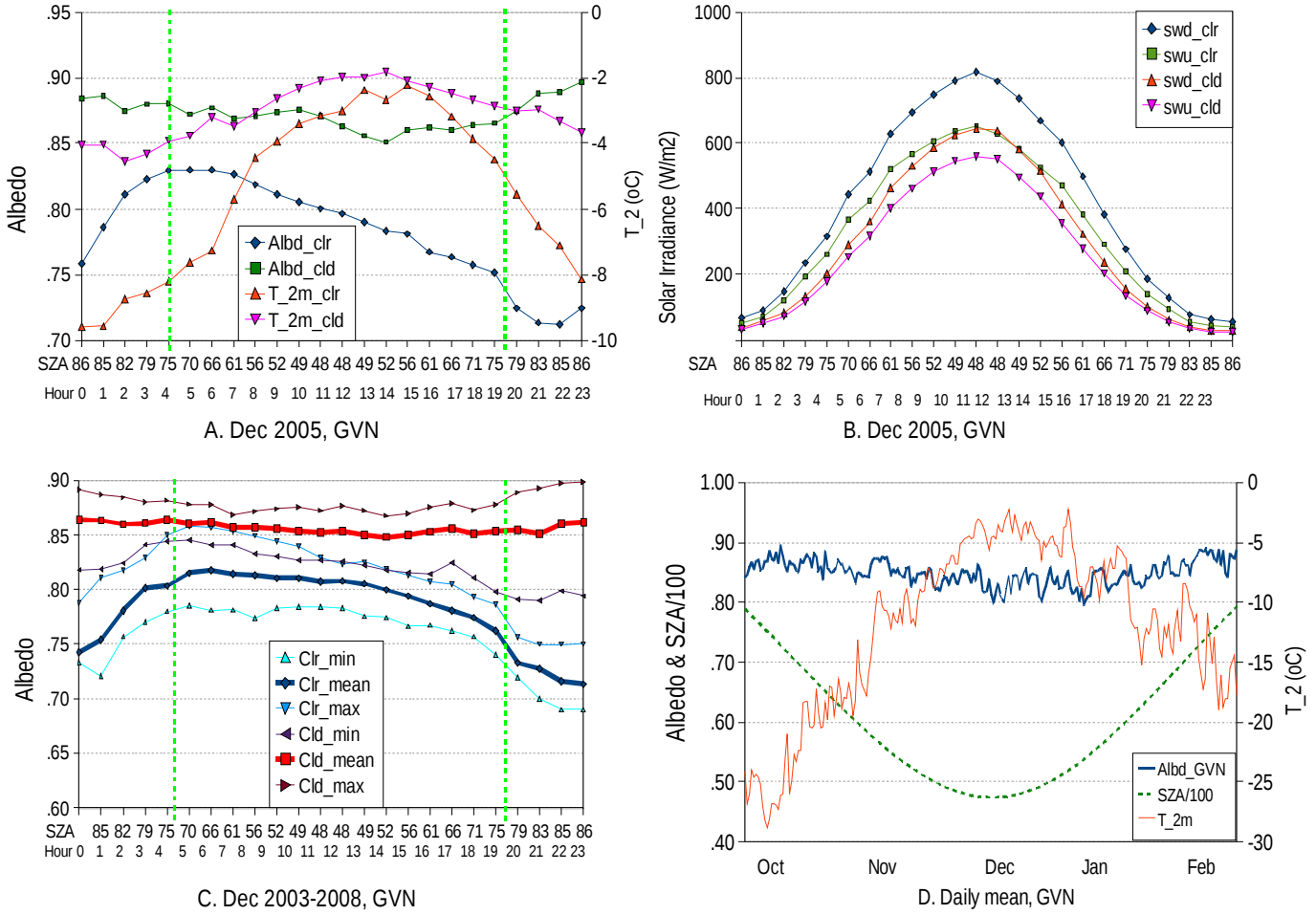

674 Figure 3. The mean diurnal cycle of snow albedo and air temperature (A) and the shortwave broadband
675 total downwelling and upwelling solar irradiance (B) for clear sky (12 days) and cloudy sky (19 days)
676 at GVN in December, 2003; the hourly mean diurnal cycle in December from 2003-2008 (C); the
677 seasonal (daily mean from 2003-2008) variation of snow albedo (D). The snow albedo values in clear
678 sky days when SZA is larger than 75° (A) beyond two vertical lines are not reliable because of the
679 pyranometer's cosine-response error at large SZAs.
680

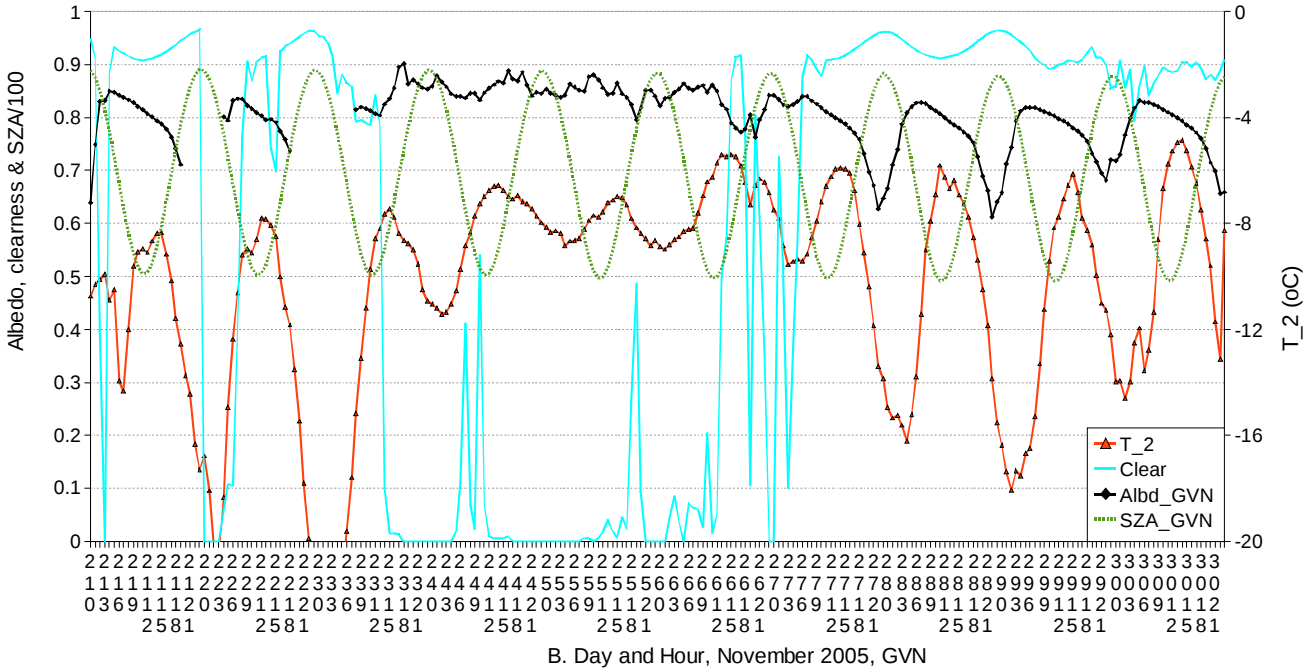

682 Figure 4. Diurnal cycles of in situ snow albedo, air temperature, and cloud index in the last ten days of
683 November, 2005, at GVN. "Clear" is the sky clearness or cloud index (0 is overcast sky, 1 is cloudless
684 sky) derived from Equation (1). The SZA on November 25 at GVN varies from 49° at solar noon to
685 88° at 0:00.

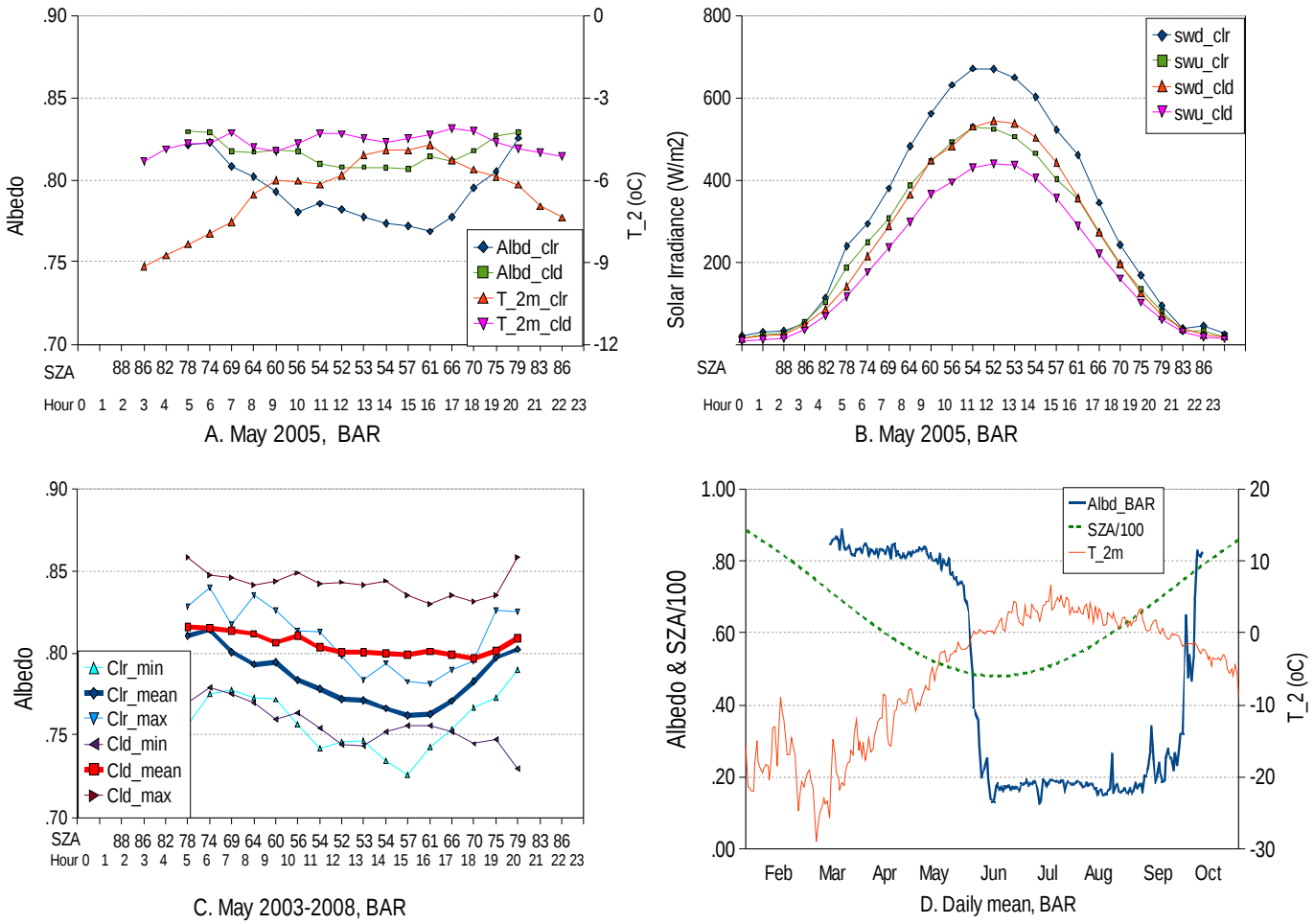

Figure 5. The mean diurnal cycle of snow albedo and air temperature (A) and the shortwave broadband total downwelling and upwelling solar irradiance (B) for clear sky (8 days) and cloudy sky (23 days) at BAR in May, 2005; the hourly mean diurnal cycle in May from 2003-2008 (C); the seasonal (daily mean from 2003-2008) variation (D).

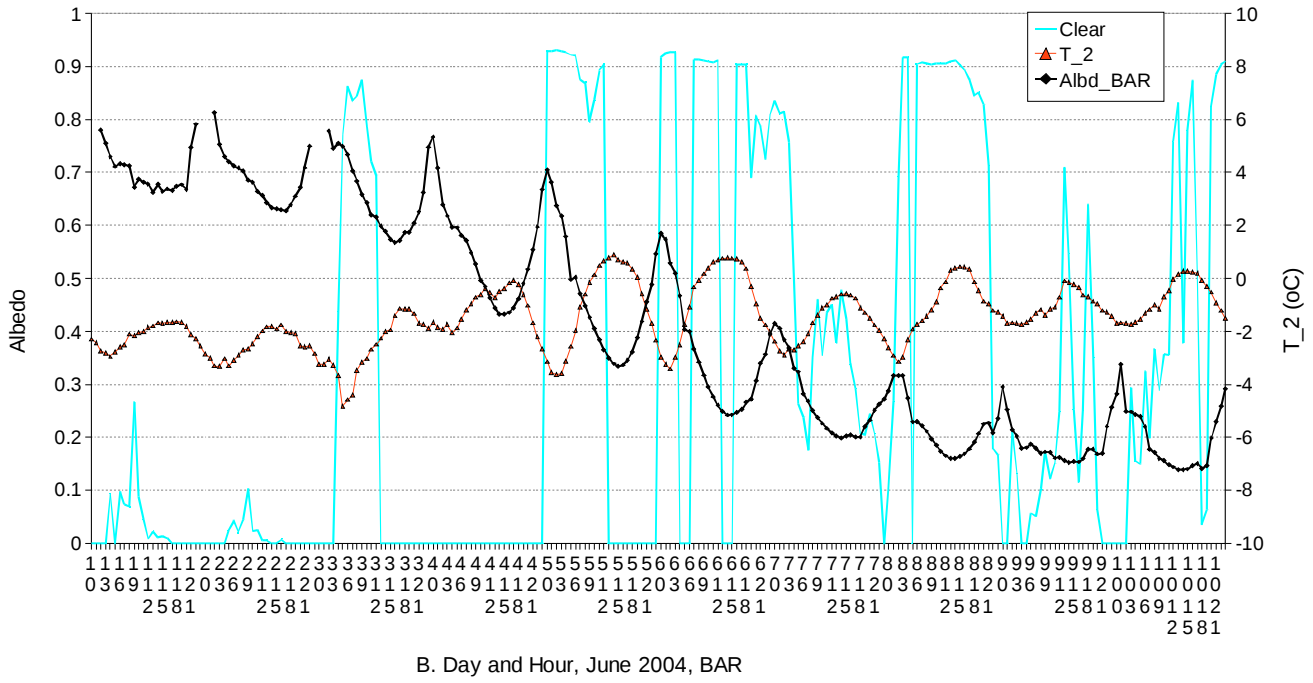

Figure 6. Diurnal cycles of in situ snow albedo, air temperature, and cloud index in the first ten days of June, 2004, at BAR. “Clear” is the sky clearness or cloud index (0 is overcast sky) derived from Equation (1). The SZA on June 5 varies from 49° at local noon to 85° at local 23:00. The sun is always above the horizon during this period.

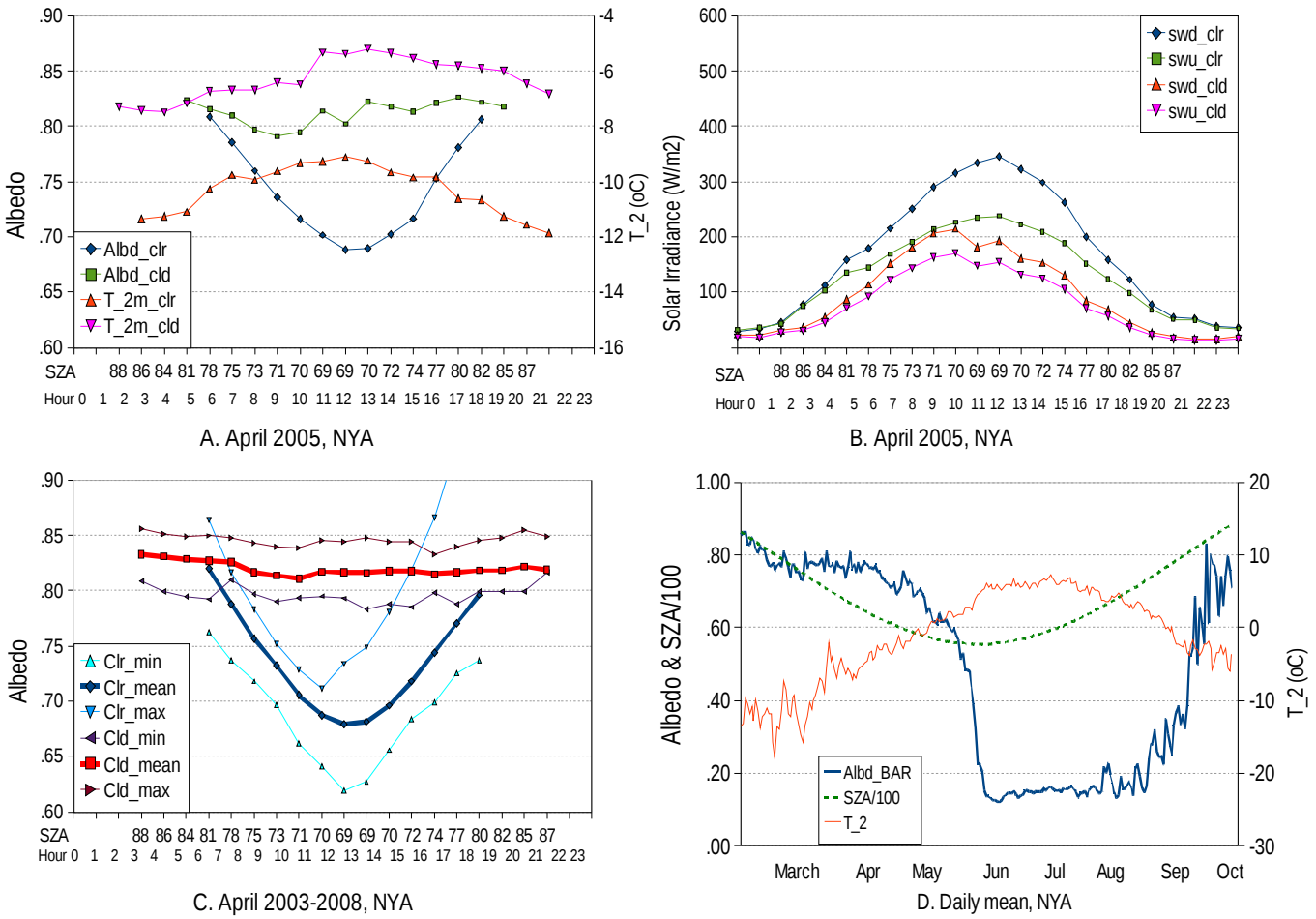

Figure 7. The mean diurnal cycle of snow albedo and air temperature (A) and the shortwave broadband total downwelling and upwelling solar irradiance (B) for clear sky (13 days) and cloudy sky (17 days) at NYA in April, 2005; the hourly mean diurnal cycle in April from 2003-2008 (C); the seasonal (daily mean from 2003-2008) variation (D), and the daily values are derived from the 24-hour period when both SWD and SWU are larger than 5 W/m^2.

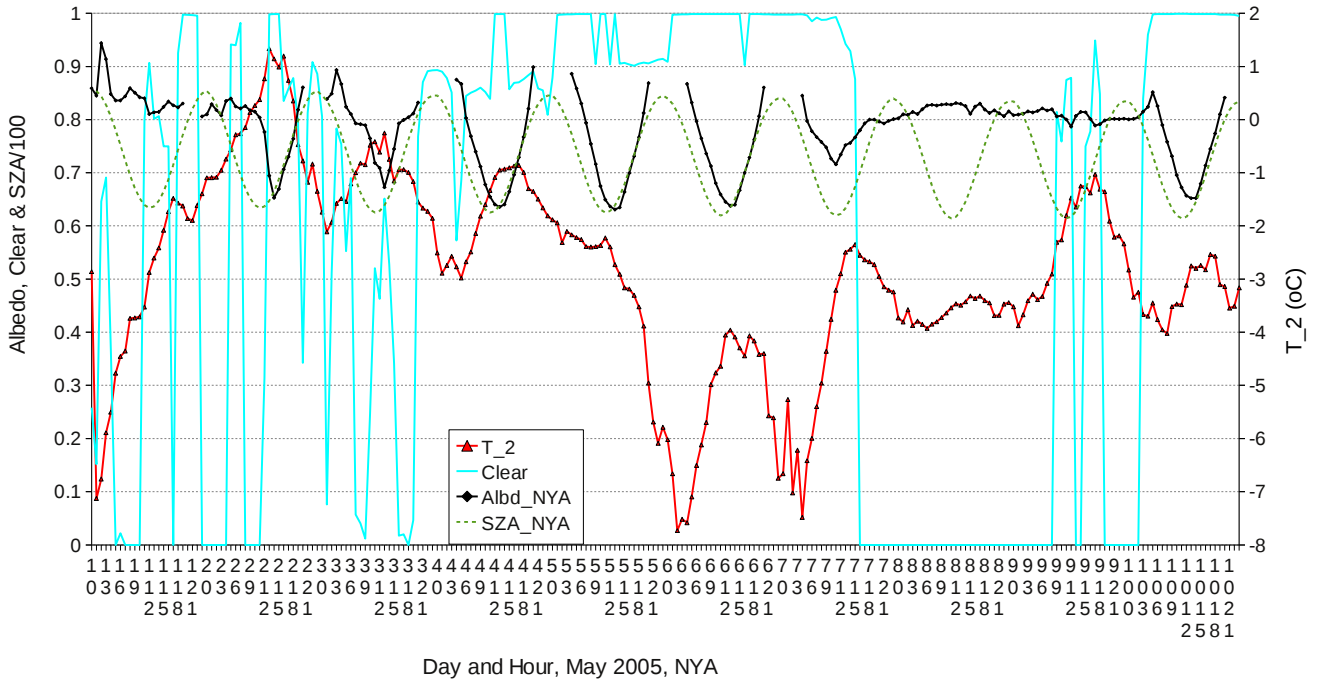

713 Figure 8. Diurnal cycles of in situ snow albedo, air temperature, and cloud index in the first ten days of
714 May, 2005, at NYA. “Clear” is the sky clearness or cloud index (0 is overcast sky) derived from
715 Equation (1). The SZA on May 5 varies from 62° at local noon to 85° at local 23:00. The sun is
716 always above the horizon during this period.
717

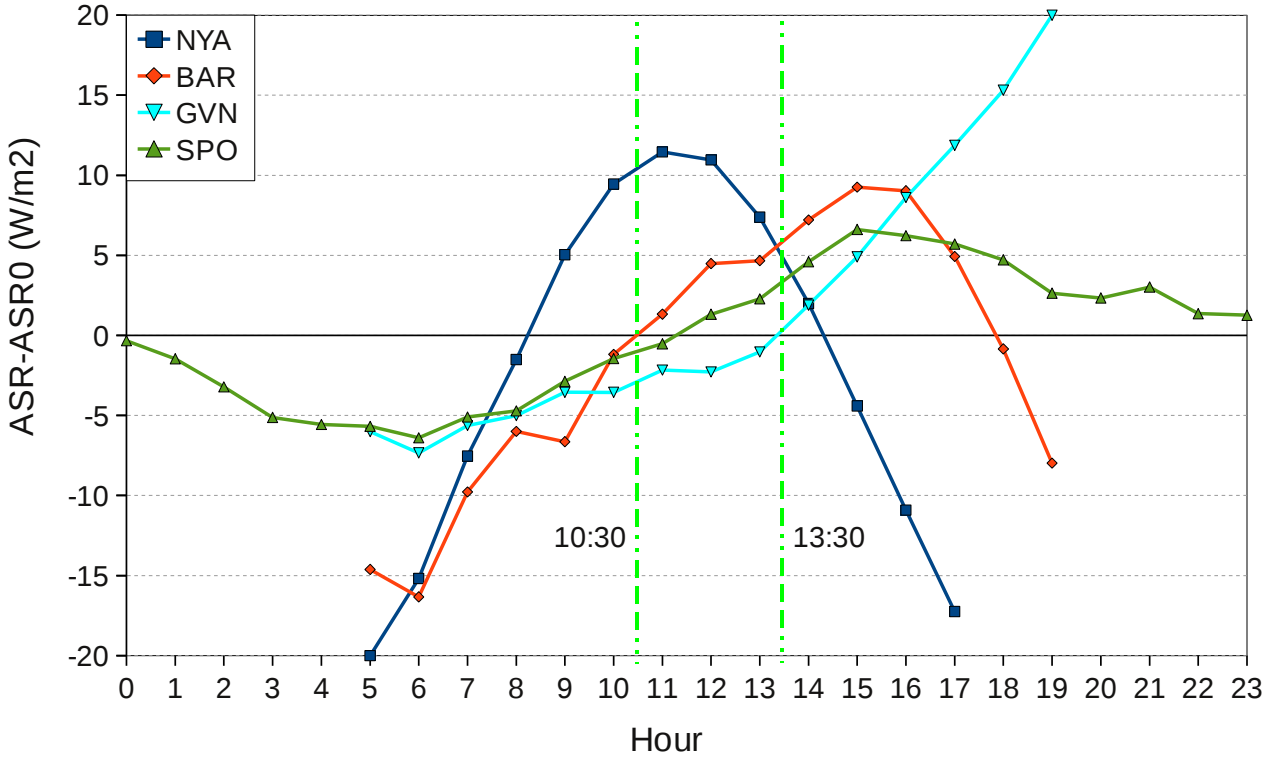

Figure 9. The difference of absorbed solar radiation (ASR) in clear-sky days on the snow surface derived from the daily mean SWD and SWU (ASR_0) and from the daily mean SWD and one instantaneous albedo within each hour, which is assumed to represent the instantaneous albedo measurement from a sun-synchronous satellite. This instantaneous albedo also represents the daily albedo to assess the ASR difference for satellite's instantaneous measurements (ASR) versus the 24-hour mean value (ASR_0). The daily mean ASR at NYA in April, BAR in May, GVN and SPO in December is 39, 65, 83 and 61 W/m^2 for clear sky, and 26, 51, 60 and 59 W/m^2 for the entire month for clear and cloudy sky, respectively (Table 2). The two vertical green lines indicate the equatorial pass time of Terra and Aqua satellites that onboard MODIS instruments.